Small-scale energy cascade in homogeneous isotropic turbulence

Mohamad Ibrahim Cheikh and James Chen*
Mechanical and Aerospace Engineering Department, University at Buffalo, The State University of New York, Buffalo, New York 14260, USA

Mingjun Wei
Mechanical and Nuclear Engineering Department, Kansas State University, Manhattan, Kansas 66506, USA

(Received 24 April 2019; published 25 October 2019)

The dynamics behind the multiscale energy transfer in turbulent flows is investigated in a numerical simulation of homogeneous isotropic turbulence (HIT). The investigation relies on conservation laws derived from the incompressible morphing continuum theory on the basis of the Boltzmann-Curtiss kinetic theory. The resulting conservation laws reveal the existence of small-scale routes for the flow of energy, which broadens the view on energy cascade (forward or inverse). The comparison of the turbulence characteristic with the reference study indicates that the turbulence features in both frameworks are equivalent at the global and small-scales; however, the presented framework shows a more detailed energy flow mechanism, while maintaining the same global dissipation rate. The study reveals that the theoretical small-scale structures can represent the small-scale structures in the turbulent flow. Finally, the energy analysis is carried out based on the presented conservation laws. The analysis reveals that at the small-scale both forward and inverse energy cascade exist in HIT; however, an overall negative energy flux (forward cascade) is present globally. Finally, the energy analysis shows that the energy cascade is highly dependent on the rotation of the small-scale structure as well as their translational motion.

DOI: 10.1103/PhysRevFluids.4.104610

I. INTRODUCTION

Turbulence remains as one of the most relevant problems in physics today. For a century, much work has been done on finding universal physical parameters that can describe the behavior of all turbulent flows [1]. Nevertheless, most of the applied turbulence models to date still lack universality [2]. This quality holds true for turbulence closure models in Large eddy simulations [3], Reynolds-averaged Navier-Stokes equations [4], and for flows in complex configurations [5]. With the rapid developments in aerospace engineering, the need for a universal turbulent model for all types of flows is apparent.

To further the understanding of turbulence, it is important to study the energy flow in both small and large-scale turbulent structures [1]. Large-scale structures are usually of the order of the flow width and contain most of the energy. They dominate the transport of mass, momentum, and internal energy. Small scales, however, are responsible for most of the energy dissipation [1]. Although theses scales can be easily defined at high Reynolds numbers [6], a certain level of ambiguity has always been persistent in flows with moderate Reynolds number [1].

*chenjm@buffalo.edu

Of the two turbulent scales, characterizations of the small-scale turbulent structures have a higher prospect of producing a universal or quasiuniversal model than the large-scale structures [1]. Taylor [7] and Betchov [8] pioneered the study on the small-scale characteristics, evolution, and contribution to the turbulent bulk flow. Their work, though limited to homogeneous turbulence, established the importance of small-scale strain amplification and vortex stretching in energy cascade.

It is not until the celebrated work of Kolmogorov's K41 theory [9], the study of the small-scale turbulent structure became a focal point in the characterization of turbulence. The first premises of the K41 theory is, at large Reynolds numbers, the average energy dissipation rate is independent of the viscosity. The second premise (known as local isotropy) is that small-scale structures at sufficiently high Reynolds numbers are statistically independent of the large-scale one. These small-scale structures are homogeneous, isotropic, and steady. In short, K41 states that the statistical properties at the dissipation scales are determined universally by the viscosity and average dissipation rate, while those at the inertial range, (at high Reynolds number), are determined by the average dissipation rate only. It implies that Richardson's multistep energy cascade process disappears at the smallest scales. The K41 theory has made remarkable predictions on the statistical properties of homogeneous and isotropic turbulence both experimentally and numerically [1]. Kolmogorov K41 theory was by far the first theory which gave a quantitative meaning for turbulence.

Although Kolmogorov's theory unveiled universal features depicting the flow of energy at the small-scale and inertial scale, these results were derived under the assumption of a globally homogeneous and isotropic turbulence. The global isotropy assumption can be relaxed, but, apparently, not the assumption of global homogeneity [10]. Zubair [11] showed that at atmospheric Reynolds numbers, large-scale structures can contribute to the energy dissipation in a much greater scale than what Kolmogorov had predicted. Vincent and Meneguzzi [12] observed that when the small-scale turbulent vortices are arranged in tube like structures, the energy cascade does not follow the traditional view described by Kolmogorov and Richardson in the inertia range. Instead, it is a one step process with a strong correlation between the small and large-scale structures. Jimenez and Wray [13] showed that the highest dissipation of kinetic energy is achieved when the small-scale structures are arranged as sheets. Horiuti [14] later showed that the topology of the sheets contributes to the magnitude of energy dissipation with flat sheets dissipating more energy than curved sheets. Even if the global homogeneous isotropy condition was satisfied, Kolmogorov's K41 was found to be inconsistent with some numerical and experimental studies [1]. Thus, the challenge of understanding the energy flow at the level of small-scale turbulence still remains.

In light of these publications, the motivation behind the present work is to analyze the flow of energy at the small-scale level. The study aims at understanding the relation between the kinematics of the small-scale structures and the energy flow. In particular, the work decouples small-scale rotational motions from the translational motions to explain the energy flow. Resorting to Navier-Stokes (NS)-based direct numerical simulations to showcase this energy flow is tedious considering the strong coupling between translational and rotational motions of the fluid. The present work is on the basis of a morphing continuum theory (MCT), a high order continuum theory. MCT incorporates small-scale structures and has their own independent degrees of freedom for translational and rotational motions [15]. These small-scale structures decouple the rotational motion from the translational motion of the flow, giving the fluid element a total of six-degrees of motion. The study assumes that the small-scale structures adopt the role of the smallest turbulent structures. The present work emphasizes the contribution of the small-scale kinematics on the energy flow in turbulence.

The current study utilizes the incompressible MCT governing equations to explore the physics of energy transfer in homogeneous isotropic turbulence (HIT), a regime where the flow shows agreement with the universal teardrop features of turbulence [16]. To accomplish this task, the study starts by giving a brief description of the morphing continuum theory, and its balance laws in dimensional and dimensionless form in Sec. II. In Sec. III, the study derives the morphing continuum

conservation laws in the framework of a translational symmetry. The conservation laws shed light on the routes that control the energy flow at small-scale. These energy routes are implemented to analyze the HIT work of Ooi *et al.* [17] in Sec. IV. The section starts by proposing a model that translates an NS case into the MCT framework, and is followed by analyzing the capability of the model in reproducing the turbulent characteristics of the reference case at the global and small scale. Finally, the study employs the newly derived energy routes derived in Sec. III to investigate the energy cascade at the level of the small-scale turbulent structures in Sec. V.

II. MORPHING CONTINUUM THEORY

A morphing continuum theory (also known as microcontinuum [18,19], microfluid [20], or generalized extended Navier-Stokes [21]), describes a continuous fluent medium composed of finite-size structures at the small scale, whose properties and behaviors affect the global motion of the fluid. A morphing continuum differs from the classical continuum which considers the space as a continuous set of volumeless points. Eringen [18,19,22,23] and De Groot and Mazur [24], the pioneers behind the theory, developed it to deal with a class of fluids which exhibit certain small-scale effects arising from the local structure and small-scale motions of the fluid elements. Most importantly, their work showed that the independent description of rotational motion (including gyration) allows capturing the small-scale structures without relying on arbitrarily fine meshes. It provides the opportunity to explore regimes where classical fluid equations break down. Recently, Wonnel and Chen [25] have formulated the governing laws of MCT under the framework of kinetic theory with Boltzmann-Curtiss distribution, and they demonstrated the correlation between the MCT and NS governing laws.

The theory has been implemented in simulating flows that diverge from NS equations, like flows in microchannels [26], lubrication theory [27], and blood flow through tapered arteries with stenosis [28]. More recently, MCT was implemented in simulating incompressible turbulence over a flat plate [29], and compressible turbulence over different types of geometries [30–32].

The current work assumes a continuum that is made up of rigid small-scale structures that retain their own rotational effects and small-scale rotational inertia [20]. The small-scale structures do not incorporate axial contractions or expansions, but compromise solely of rotational motion about their center of mass. The small-scale structures are considered to be rigid spherical structures with constant material properties. Thus, the inertia of these structures (j) has the relation $j = \frac{2}{5}r^2$, where r represents the radius of a sphere [33]. The motion variables that control the behavior of the small-scale structures are the translational velocity v_k, and the gyration, ω_k which characterizes the local rotation of these structures. From the aforementioned variables, one can see that the kinetic energy of the flow is two folds; the classical translational kinetic energy ($\frac{1}{2}v_i v_i$) and a new form of kinetic energy that is characterized by the gyration of the small-scale structures called the rotational kinetic energy ($\frac{1}{2}j\omega_i\omega_i$) [33]. The resultant deformation rate tensors that govern the behavior of a morphing continuum flow are [15,34]

$$a_{kl} = v_{l,k} + \varepsilon_{lkm}\omega_m, \tag{1}$$

$$b_{kl} = \omega_{k,l}, \tag{2}$$

where a_{kl} resembles the classical deformation-rate tensor from the Navier-Stokes equations with an additional term representing the effect of the gyration of the small-scale structures. The b_{kl} tensor is a new deformation tensor not found in the classical fluid theory, representing the strain and rotation gradients experienced by gradients of the gyration [15].

A. Balance laws

With the aforementioned deformation rate tensors, the linear constitutive equations can be derived from Clausius-Duhem inequality [15,22]. By inserting the constitutive equations into the

thermodynamic balance laws, the morphing continuum governing equations for incompressible fluids can be found as

conservation of mass:

$$v_{m,m} = 0, \tag{3}$$

Balance of linear momentum:

$$\frac{Dv_m}{Dt} = -\frac{p_{,m}}{\rho} + \frac{(\mu+\kappa)}{\rho} v_{m,nn} + \frac{\kappa}{\rho}\varepsilon_{mnk}\omega_{k,n} + F_m, \tag{4}$$

Balance of angular momentum:

$$\frac{D\omega_m}{Dt} = \frac{(\alpha+\beta)}{j\rho}\omega_{l,lm} + \frac{\gamma}{\rho j}\omega_{m,nn} + \frac{\kappa}{\rho j}(\varepsilon_{mnk}v_{k,n} - 2\omega_m) + L_m, \tag{5}$$

Balance of internal energy:

$$\begin{aligned}\frac{De}{Dt} = &-\frac{p}{\rho}v_{k,k} + \frac{\mu}{\rho}(v_{l,k}+v_{k,l})v_{l,k} + \frac{\kappa}{\rho}(v_{l,k}v_{l,k} - 2\omega_m\varepsilon_{mkl}v_{l,k} + 2\omega_m\omega_m)\\ &+ \frac{\alpha}{\rho}\omega_{m,m}\omega_{k,k} + \frac{\beta}{\rho}\omega_{k,l}\omega_{l,k} + \frac{\gamma}{\rho}\omega_{l,k}\omega_{l,k} - \frac{q_{k,k}}{\rho},\end{aligned} \tag{6}$$

Clausius-Duhem inequality:

$$\begin{aligned}&-\left(\frac{D\psi}{Dt} + \eta\frac{D\theta}{Dt}\right) + \frac{\mu}{\rho}(v_{l,k}+v_{k,l})v_{l,k} + \frac{\kappa}{\rho}(v_{l,k}v_{l,k} - 2\omega_m\varepsilon_{mkl}v_{l,k} + 2\omega_m\omega_m) + \frac{\alpha}{\rho}\omega_{m,m}\omega_{k,k}\\ &+ \frac{\beta}{\rho}\omega_{k,l}\omega_{k,l} + \frac{\gamma}{\rho}\omega_{l,k}\omega_{k,l} - \frac{q_k}{\rho\theta}\theta_{,k} \geqslant 0,\end{aligned} \tag{7}$$

where ρ is the fluid density, q_k is the heat flux, ψ is Helmholtz free energy density, θ is absolute temperature, e is the internal energy density, p is the hydrostatic pressure, j is the inertia of the small-scale structures, μ is the dynamic viscosity, κ is the rotational viscosity (also called the coupling coefficient between the linear and angular momenta [33]), γ is the gyration diffusion coefficient, and α and β are viscous coefficients related to the gyration. F_m and L_m are the large-scale forcing and large-scale torque divided by the density, and added to the momentum equations, respectively.

B. Balance laws in dimensionless form

The current subsection dimensionalizes the MCT balance laws with the dimensionless groups defined based on the physical parameters of interest. Only the continuity and momentum balance laws are nondimensionalized. Starting with the distance and motion variables, the length scales x_m, and the translation velocity v_m are parameterized with the root-mean-square velocity v_{rms}, and the Taylor microscale λ defined as [17]

$$\lambda = \sqrt{\frac{\langle v_p v_p\rangle}{\langle v_{i,i}v_{j,j}\rangle}}, \tag{8}$$

where $\langle ...\rangle$ is the volume average over the computational domain. In this regard, normalizing the balance laws with the Taylor microscale leads to the dimensionless form, i.e.,

Dimensionless linear momentum equation:

$$\frac{\partial(\hat{\mathbf{v}})}{\partial\hat{t}} + \hat{\mathbf{v}}\cdot\hat{\nabla}\hat{\mathbf{v}} = -\hat{\nabla}\hat{p} + \frac{1}{\text{Re}_\lambda}\hat{\nabla}^2\hat{\mathbf{v}} + \frac{1}{\text{Er}_\lambda}(2\hat{\nabla}\times\hat{\boldsymbol{\omega}} + \hat{\nabla}^2\hat{\mathbf{v}}) + \mathcal{F}_m, \tag{9}$$

Dimensionless angular momentum equation:

$$\frac{\partial(\hat{\boldsymbol{\omega}})}{\partial \hat{t}} + \hat{\mathbf{v}} \cdot \hat{\nabla}\hat{\boldsymbol{\omega}} = \frac{1}{C_\lambda^{\alpha\beta}}\hat{\nabla}(\hat{\nabla} \cdot \hat{\boldsymbol{\omega}}) + \frac{1}{C_\lambda^{\gamma}}\hat{\nabla}^2\hat{\boldsymbol{\omega}} + \frac{\mathcal{D}}{\mathrm{Er}_\lambda}(\hat{\nabla} \times \hat{\mathbf{v}} - 2\hat{\boldsymbol{\omega}}) + \mathcal{L}_m, \tag{10}$$

where $\mathcal{D} = 2\lambda^2/j = 5(\lambda/r)^2$ represents the square ratio of the Taylor microscale, to the radius of the MCT small-scale structures. This parameter illustrates one of the biggest advantage of MCT over classical fluid theory, namely, the ability to probe the physics of the smallest length scale without the need for extremely fine grids, or *ad hoc* models [29,35].

One of the nondimensional variables that appears in the governing equations is the MCT Taylor Reynolds number, which measures the ratio of the inertial forces to the viscous forces. In the current work, $\mu + \kappa/2$ is used to represent the viscous forces, due to the fact that it will appears in the dissipation term of the total kinetic energy (ε) in Sec. III. Earlier work used $\mu + \kappa$ to represent the viscous forces [35]; however, after deriving the energy routes in Sec. III, it became apparent that only $\mu + \kappa/2$ contributes to the total kinetic energy dissipation, while the remaining $\kappa/2$ contributes to energy loss through the MCT enstrophy. Consequently, the Taylor-Reynolds number is

$$\mathrm{Re}_\lambda = \frac{\rho v_{\mathrm{rms}}\, \lambda}{\mu + \kappa/2}. \tag{11}$$

The next three dimensionless terms are Eringen's number Er in honor of Eringen, $C_\lambda^{\alpha\beta}$ a dimensionless parameter that governs the gyration viscous coefficients and C_λ^{γ} a dimensionless parameter that governs the diffusion of the gyration,

$$\mathrm{Er}_\lambda = \frac{\rho v_{\mathrm{rms}}\, \lambda}{\kappa/2}, \quad C_\lambda^{\alpha\beta} = \frac{\rho v_{\mathrm{rms}} \lambda j}{\alpha + \beta}, \quad C_\lambda^{\gamma} = \frac{\rho v_{\mathrm{rms}} \lambda j}{\gamma}. \tag{12}$$

III. CONSERVATION LAWS FOR INCOMPRESSIBLE FLUIDS

Ever since the work of Arnold *et al.* [36] on two- and three-dimensional incompressible flows, it has been shown that the Eulerian form of the governing equations for many fluid systems can be expressed as an infinite-dimensional, generalized Hamiltonian dynamical system [37]. Such expression permits the use of analytical mechanics, in particular Noether's theorem. This theory states that for each conservation law there exists an adjacent variational symmetry associated with the law itself [38]. Following Noether's theorem, theoretical physicists tended to combine conservation laws with symmetry. For example, the momentum conservation law in classical fluid theory corresponds to the symmetry of space translation, $x(t, \vec{r}) = x(t, \vec{r} + \vec{p})$ [10].

The current section derives the conservation laws for an incompressible flow by utilizing the the symmetry of spatial translation, which assumes periodic boundary conditions over the whole domain. The study assumes smoothness of the velocity, gyration, and pressure fields to permit any differential manipulations of the said fields. All source terms in the governing equations are nullified, and all variables are averaged over the whole domain where the angular brackets are denoted for the volume average,

$$\langle f \rangle = \frac{1}{R^3}\int_{B_R} f(\vec{r}) d\vec{r}, \tag{13}$$

where $f(\vec{r})$ is an arbitrary periodic function, B_R is the domain boundary, and R is the domain width. Some useful identities can be found in the book by Frisch [10].

In the following sections the word "global" references the volume average ($\langle ... \rangle$), and the word "local" refers to the unaveraged or total field. Thus, "local" is for a single point while "global" is for the whole domain. Since MCT assumes the continuum to be comprised of small-scale structures, every point is associated with a small structure. So the local scale in this regard becomes equivalent to the MCT small-scale structure.

A. Conservation of linear momentum

Conservation of linear momentum is derived by applying spatial averaging over the incompressible linear momentum balance [Eq. (4)] as

$$\frac{d\langle v_m\rangle}{dt} = -\frac{\langle p_{,m}\rangle}{\rho} + \frac{\mu+\kappa}{\rho}\langle v_{m,nn}\rangle + \frac{\kappa}{\rho}\langle \varepsilon_{mln}\omega_{n,l}\rangle. \tag{14}$$

All the spatial derivatives of a periodic function in the linear momentum equation are dropped after spatial averaging. The final form of the conservation of linear momentum equation is

$$\frac{d\langle v_m\rangle}{dt} = 0. \tag{15}$$

This signifies that the linear momentum is conserved in MCT, similar to results obtained in the classical fluid theory [10].

B. Conservation of angular momentum

Similarly, the conservation of angular momentum is derived by applying spatial averaging over the angular momentum,

$$\frac{d\langle \omega_m\rangle}{dt} = \frac{(\alpha+\beta)}{j\rho}\langle \omega_{l,lm}\rangle + \frac{\gamma}{j\rho}\langle \omega_{m,ll}\rangle + \frac{\kappa}{j\rho}\langle \varepsilon_{mln}v_{n,l} - 2\omega_m\rangle. \tag{16}$$

By removing all the spatial derivatives, the equation becomes

$$\frac{d\langle \omega_m\rangle}{dt} = -\frac{2\kappa}{\rho j}\langle \omega_m\rangle. \tag{17}$$

From the equation, one can see that the angular momentum is not conserved, but decays with a characteristic time constant $\tau^{\omega} = \frac{\rho j}{2\kappa}$. This is inconsistent with the definition of conservation of angular momentum, which requires that $d\langle \omega_m\rangle/dt = 0$. Thus, to ensure conservation of angular momentum, the mean gyration $\langle \omega_m\rangle$ of the system should equal to zero, or the local vorticity of the flow should equal to twice the gyration ($\varepsilon_{mln}v_{n,l} = 2\omega_m$).

Such a concept of relaxation time has been reported in the extended Kinetic theory [39]. Kinetic theory describes many systems that diverge from their equilibrium state, and one of the most famous equations that model such systems is the BGK model of the Boltzmann's equation [39]. The BGK model replaces the nonlinear collision term of the Boltzmann equation by a simpler term that describes molecular interaction by introducing a characteristic time scale τ^{BGK}. The characteristic time scale in the BGK model represents weak departure from the local equilibrium, and has long been recognized as a good approximation [40]. One approximation to the characteristic time τ^{BGK}, is to use the turbulence relaxation time τ^{turb} for the departure from local equilibrium due to turbulent eddy interactions and their inhomogeneity in the main flow [41]. Following this logic, the derived τ^{ω} could be used as a turbulence relaxation time, since it represents the decay time of the rotational speed of the turbulent eddies.

C. Conservation of energy

The kinetic energy in MCT is decomposed into translation ($\frac{1}{2}v_iv_i$) and rotation ($\frac{1}{2}j\omega_i\omega_i$) components [33]. The decoupled kinetic energy routes in global scales can be found in Fig. 1. The translational kinetic energy can be derived by multiplying the balance law of linear momentum [Eq. (4)] by the velocity,

$$\frac{1}{2}\frac{d(v_mv_m)}{dt} = -\frac{p_{,k}v_m}{\rho} + \frac{(\mu+\kappa)}{\rho}v_{m,kk}v_m\frac{\kappa}{\rho}v_m\varepsilon_{mlk}\omega_{l,k}. \tag{18}$$

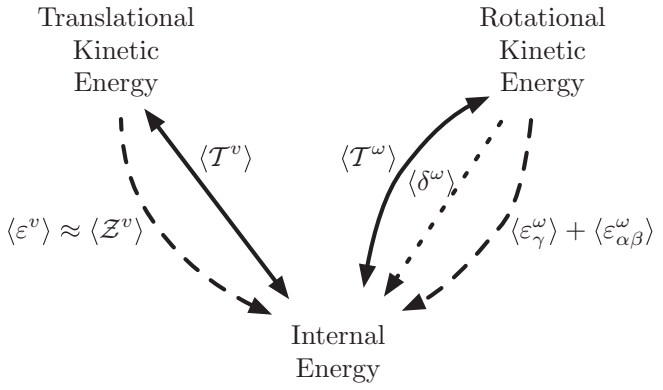

FIG. 1. Global energy routes.

Applying spatial averaging over Eq. (18) yields the average conservation of the translational kinetic energy,

$$\frac{1}{2}\frac{d\langle v_m v_m\rangle}{dt} = \frac{\mu+\kappa}{\rho}\langle v_m v_{m,nn}\rangle + \frac{\kappa}{\rho}\langle v_m(\varepsilon_{mln}\omega_{n,l})\rangle. \tag{19}$$

This equation is similar to the Navier-Stokes conservation of energy [10], but contains an extra term on the right-hand side. The first term on the right-hand side can be expanded as the mean dissipation rate of the translational motion $\langle \varepsilon^v \rangle$,

$$\frac{1}{2}\frac{d\langle v_m v_m\rangle}{dt} = \underbrace{-\frac{\mu+\kappa}{2\rho}\langle (v_{k,j}+v_{j,k})(v_{k,j}+v_{j,k})\rangle}_{\langle \varepsilon^v \rangle} + \underbrace{\frac{\kappa}{\rho}\langle v_m(\varepsilon_{mln}\omega_{n,l})\rangle}_{\langle \mathcal{T}^v \rangle}, \tag{20}$$

where the local translation dissipation rate is

$$\varepsilon^v = \frac{\mu+\kappa}{2\rho}(v_{k,j}+v_{j,k})(v_{k,j}+v_{j,k}). \tag{21}$$

Instead of expanding the first term to get the mean translational dissipation term $\langle \varepsilon^v \rangle$, one can expand it to get the mean enstrophy $\langle \mathcal{Z}^v \rangle$ as

$$\frac{1}{2}\frac{d\langle v_m v_m\rangle}{dt} = -2\frac{\mu+\kappa}{\rho}\underbrace{\left\langle \frac{1}{2}\varepsilon_{ijk}v_{k,j}\varepsilon_{imn}v_{n,m}\right\rangle}_{\langle \mathcal{Z}^v \rangle} + \underbrace{\frac{\kappa}{\rho}\langle v_m(\varepsilon_{mln}\omega_{n,l})\rangle}_{\langle \mathcal{T}^v \rangle}, \tag{22}$$

where the local enstrophy is

$$\mathcal{Z}^v = \tfrac{1}{2}\varepsilon_{ijk}v_{k,j}\varepsilon_{imn}v_{n,m}. \tag{23}$$

Both the mean enstrophy and mean translational dissipation rate are equivalent at the global scale, but at the local scale they are related by the pressure Poisson equation as

$$\mathcal{Z}^v - \frac{\rho}{2(\mu+\kappa)}\varepsilon^v = \frac{p_{,mm}}{\rho}. \tag{24}$$

As for the second term on the right-hand side,

$$\mathcal{T}^v = \frac{\kappa}{\rho}v_m(\varepsilon_{mln}\omega_{n,l}), \tag{25}$$

it represents the local energy transferred in or out of the translation kinetic energy through gyration. This term represents the impact of the gyration on the energy flow of the translational kinetic energy equation. One should note that this term does not mean that the translational energy is taking or giving energy to the rotational energy, it only means that the existence of the gyration impacts the translational kinetic energy either by injection or ejection regardless of the source.

The rotational kinetic energy component ($\frac{1}{2} j\omega_i\omega_i$) is derived by multiplying the balance law of angular momentum [Eq. (5)] by the gyration,

$$\frac{1}{2}\frac{d(j\omega_m\omega_m)}{dt} = \frac{(\alpha+\beta)}{j\rho}\omega_{l,lm}\omega_m + \frac{\gamma}{\rho}\omega_{m,ll}\omega_m + \frac{\kappa}{\rho}(\varepsilon_{mlk}v_{k,l}\omega_m - 2\omega_m\omega_m). \tag{26}$$

Applying spatial averaging over Eq. (26) yields the mean conservation of rotational energy,

$$\frac{j}{2}\frac{d\langle\omega_m\omega_m\rangle}{dt} = \underbrace{-\frac{(\alpha+\beta)}{j\rho}\langle\omega_{l,l}\omega_{m,m}\rangle}_{\langle\varepsilon^{\omega}_{\alpha\beta}\rangle} \underbrace{-\frac{\gamma}{\rho}\langle\omega_{m,l}\omega_{m,l}\rangle}_{\langle\varepsilon^{\omega}_{\gamma}\rangle} + \underbrace{\frac{\kappa}{\rho}\langle\omega_m(\varepsilon_{mln}v_{n,l})\rangle}_{\langle\mathcal{T}^{\omega}\rangle} \underbrace{-2\frac{\kappa}{\rho}\langle\omega_m\omega_m\rangle}_{\langle\delta^{\omega}\rangle}. \tag{27}$$

Similar to the translational energy, the first two terms on the right-hand side represent the mean of the rotational dissipation terms,

$$\varepsilon^{\omega}_{\alpha\beta} = \frac{\alpha+\beta}{\rho}\omega_{m,m}\omega_{l,l}, \quad \varepsilon^{\omega}_{\gamma} = \frac{\gamma}{\rho}\omega_{m,l}\omega_{m,l}. \tag{28}$$

The first term ($\varepsilon^{\omega}_{\alpha\beta}$) measures the dissipation of rotational kinetic energy due to the expansion or contraction of the gyration. The second term ($\varepsilon^{\omega}_{\gamma}$) measures the mechanical dissipation of rotational kinetic energy due to friction between adjacent gyrations. The last term (δ^{ω}) represents the small-scale decay of the rotational energy, i.e.,

$$\delta^{\omega} = 2\frac{\kappa}{\rho}\omega_m\omega_m. \tag{29}$$

This term is also associated with the time constant τ^{ω} which governs the decay of angular momentum in MCT as shown in Eq. (17). Therefore, δ^{ω} is a decay term, not a dissipative term. The difference between the dissipation terms ($\varepsilon^{\omega}_{\alpha\beta}$ and $\varepsilon^{\omega}_{\gamma}$) and the decay term ($\delta^{\omega}$) is that the dissipation terms cause a loss of rotational kinetic energy through the gradient of the local motion. Therefore, if the local rotational motion (ω_m) is constant throughout the whole domain, then $\varepsilon^{\omega}_{\alpha\beta}$ and $\varepsilon^{\omega}_{\gamma}$ are zero. However, δ^{ω} measures the energy loss from the rotational motion until rotation equilibrium is achieved.

The only term left in Eq. (27) is

$$\mathcal{T}^{\omega} = \frac{\kappa}{\rho}\omega_m(\varepsilon_{mln}v_{n,l}). \tag{30}$$

This term represents the small-scale energy transferred in or out of the rotational kinetic energy by the curl of the velocity (vorticity). Note that both $\mathcal{T}^{v}$ and $\mathcal{T}^{\omega}$ are equal on average, i.e.,

$$\langle\mathcal{T}^{v}\rangle = \langle\mathcal{T}^{\omega}\rangle, \tag{31}$$

indicating that they transfer equal amounts of energy to both forms of the kinetic energy in the same quantity. On the local scale, these components are related by the equation

$$\frac{\kappa}{\rho}(\varepsilon_{mln}\omega_l v_n)_{,m} = \mathcal{T}^{v} - \mathcal{T}^{\omega}, \tag{32}$$

where the spatial average of $(\varepsilon_{mln}\omega_l v_n)_{,m}$ is zero, leading it to vanish at the global scale. On the local scale, however, $\frac{\kappa}{\rho}(\varepsilon_{mkl}\omega_k v_l)_{,m}$ controls the direction of energy flow, either to the translational or rotational component of the kinetic energy. If $\frac{\kappa}{\rho}(\varepsilon_{mkl}\omega_k v_l)_{,m}$ is positive, then the translational component gains kinetic energy, and the rotational component loses it. Another way to understand

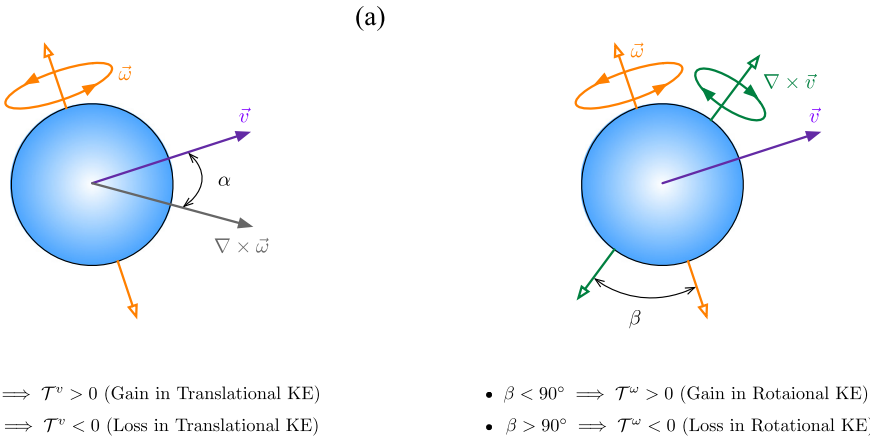

FIG. 2. Sketch showing the kinematics of the small-scale structures. (a) Motions that govern the sign of $\mathcal{T}^v$ and (b) motions that govern the sign of $\mathcal{T}^\omega$.

how $\frac{\kappa}{\rho}(\varepsilon_{mkl}\omega_k v_l)_{,m}$ works is to look at the motion of the small-scale structures. If the curl of the gyration ($\nabla \times \vec{\omega}$) is generating a translational motion along the direction of the velocity (i.e., $\alpha < 90$), then energy is injected into the translational motion as shown in Fig. 2(a). However, if the resultant translation caused by the curl of the gyration is opposing the velocity of the small-scale structure, then the translational energy is lost as heat. Similarly, $\mathcal{T}^\omega$ has the capability of giving rise to both forms of energy transfer. If the vorticity is generating a rotational motion in the same sense of the gyration (i.e., $\beta < 90$), then energy is injected into the rotational motion motion as shown in Fig. 2(b). However, if the vorticity is opposing the gyration of the small-scale structure (i.e., $\beta > 90$), then the rotational kinetic energy is lost as heat.

By decoupling the rotational energy from the translational energy, the detailed interaction between the two is revealed. In the translational kinetic energy, i.e., Eq. (19), It can be seen that the existence of an additional energy routes that inject energy through $\mathcal{T}^v$. As for the rotational kinetic energy, it contains its own terms for the injecting, decaying and dissipating energy in the system.

To ensure conservation of total energy, all the kinetic energy that was lost or gained by the translational or rotational kinetic energy should appear in the conservation of internal energy. Applying spatial averaging over the internal energy [Eq. (6)] yields

$$\frac{d\langle e\rangle}{dt} = \langle \varepsilon^v\rangle - \langle \mathcal{T}^v\rangle - \langle \mathcal{T}^\omega\rangle + \langle \delta^\omega\rangle + \langle \varepsilon^\omega_{\alpha\beta}\rangle + \langle \varepsilon^\omega_\gamma\rangle. \tag{33}$$

All the terms that attribute to the rate of change of the translational or rotational kinetic energy are found in the conservation of internal energy but with opposite signs. This confirms the conservation of total energy in the system. The global picture of energy transfer is shown in Fig. 1. The figure reveals two different kind of routes of the energy flow. The first routes are unidirectional, i.e., one-way arrow. These routes refer to the dissipative and decay terms (δ^ω, $\varepsilon^\omega_{\alpha\beta}$, $\varepsilon^\omega_\gamma$, and ε^v). The second routes are multidirectional routes, and they represent the transfer terms ($\mathcal{T}^v$ and $\mathcal{T}^\omega$). The multidirectional routes couple the energy flow between the rotational and translation kinetic energies.

The spatial average of Clausius-Duhem inequality [Eq. (7)] is examined to ensure thermodynamical consistency, i.e.,

$$-\left\langle \frac{d\psi}{dt} + \eta\frac{d\theta}{dt}\right\rangle + \langle \varepsilon^v\rangle - \langle \mathcal{T}^v\rangle - \langle \mathcal{T}^\omega\rangle + \langle \delta^\omega\rangle + \langle \varepsilon^\omega_{\alpha\beta}\rangle + \langle \varepsilon^\omega_\gamma\rangle \geqslant 0. \tag{34}$$

One can see that there is no constraint on the routes that dissipate or decays energy ($\langle\delta^{\omega}\rangle$, $\langle\varepsilon^{\omega}_{\alpha\beta}\rangle$, $\langle\varepsilon^{\omega}_{\gamma}\rangle$, and $\langle\varepsilon^{v}\rangle$) at steady state. The second law only constrains the two multidirectional routes $\langle\mathcal{T}^{v}\rangle$ and $\langle\mathcal{T}^{\omega}\rangle$. From Eq. (34), one can see that at steady state $\langle\mathcal{T}^{v}\rangle$ and $\langle\mathcal{T}^{\omega}\rangle$ have an upper limit for injecting energy into the translational or rotational components of the kinetic energy. The upper limit is equal to the summation of the other four routes ($\langle\delta^{\omega}\rangle$, $\langle\varepsilon^{\omega}_{\alpha\beta}\rangle$, $\langle\varepsilon^{\omega}_{\gamma}\rangle$, and $\langle\varepsilon^{v}\rangle$). If the two multidirectional routes $\langle\mathcal{T}^{v}\rangle$ and $\langle\mathcal{T}^{\omega}\rangle$ are ejecting kinetic energy, then there is no constraint on them.

To compare the conservation of energy between the classical fluid theory and morphing continuum, one has to look at the total kinetic energy ($KE = \frac{1}{2}u_i u_i + \frac{1}{2}j\omega_i\omega_i$). Equations (19) and (27) describe the transfer of energy in the translational and rotational components of the kinetic energy. The MCT conservation law for the total kinetic energy is derived by adding Eqs. (18) and (26), followed by a spatial averaging,

$$\frac{d\langle KE\rangle}{dt} = \langle\mathcal{T}^{v}\rangle + \langle\mathcal{T}^{\omega}\rangle - \langle\varepsilon^{v}\rangle - \langle\delta^{\omega}\rangle - \left\langle\varepsilon^{\omega}_{\alpha\beta}\right\rangle - \left\langle\varepsilon^{\omega}_{\gamma}\right\rangle. \tag{35}$$

From the above equation one can see that there are four terms that eject kinetic energy: $\langle\varepsilon^{v}\rangle$, $\langle\varepsilon^{\omega}_{\alpha\beta}\rangle$, $\langle\varepsilon^{\omega}_{\gamma}\rangle$, and $\langle\delta^{\omega}\rangle$; and two terms that may inject or eject kinetic energy: $\langle\mathcal{T}^{v}\rangle$ and $\langle\mathcal{T}^{\omega}\rangle$. Combining $\langle\mathcal{T}^{v}\rangle$, $\langle\mathcal{T}^{\omega}\rangle$, and $\langle\delta^{\omega}\rangle$, the conservation of total kinetic energy becomes

$$\frac{d\langle KE\rangle}{dt} = \underbrace{-\frac{\mu+\kappa/2}{2\rho}\langle(v_{l,k}+v_{k,l})(v_{l,k}+v_{k,l})\rangle}_{\langle\varepsilon^{V}\rangle} \underbrace{-\left(\frac{\alpha+\beta}{\rho}\langle\omega_{m,m}\omega_{l,l}\rangle + \frac{\gamma}{\rho}\langle\omega_{l,n}\omega_{l,n}\rangle\right)}_{\langle\varepsilon^{\Omega}\rangle}$$
$$\underbrace{-\frac{\kappa}{\rho}\left(\frac{1}{2}\left\langle\Omega^{a}_{m}\Omega^{a}_{m}\right\rangle\right)}_{\left\langle\mathcal{Z}^{\Omega}\right\rangle}, \tag{36}$$

where $\Omega^{a}_{m} = \varepsilon_{lkm}v_{m,k} - 2\omega_l$ is the absolute rotation field, $\mathcal{Z}^{\Omega} = \frac{1}{2}\Omega^{a}_{m}\Omega^{a}_{m}$ is the MCT enstrophy. The absolute rotation is a relativistic field that measures the difference in rotational speed between the gyration and the vorticity [42]. The total local rotational dissipation is $\varepsilon^{\Omega} = \varepsilon^{\omega}_{\gamma} + \varepsilon^{\omega}_{\alpha\beta}$.

The local translational dissipation rate of the total kinetic energy becomes

$$\varepsilon^{V} = \frac{\mu+\kappa/2}{2\rho}(v_{k,j}+v_{j,k})(v_{k,j}+v_{j,k}). \tag{37}$$

The relationship between the local translational dissipation of the total kinetic energy ε^{V} and the local translational dissipation of the translational kinetic energy ε^{v} is

$$\varepsilon^{V} = \varepsilon^{v} + \frac{\kappa}{4\rho}(v_{k,j}+v_{j,k})(v_{k,j}+v_{j,k}). \tag{38}$$

Equation (36) shows that although both translational and rotational kinetic energies have terms that could inject energy into them ($\mathcal{T}^{\omega}$ and $\mathcal{T}^{v}$), the global flow of the total kinetic energy is always dissipative, similar to the classical fluid theory [10]. Equation (36) can be further reduced down if the conservation of angular momentum is conserved by enforcing the small-scale vorticity to be equivalent to twice the gyration ($2\omega_m = \varepsilon_{mln}v_{n,l}$). In that case, both the absolute rotation (Ω^{a}_{m}) and the MCT enstrophy ($\mathcal{Z}^{\Omega}$) become null, and the conservation of total kinetic energy becomes

$$\frac{d\langle KE\rangle}{dt} = -\frac{\mu+\kappa/2}{2\rho}\langle(v_{k,j}+v_{j,k})(v_{k,j}+v_{j,k})\rangle - \frac{\gamma}{4\rho}\langle v_{j,ii}v_{j,ll}\rangle. \tag{39}$$

One can see that the MCT conservation of total kinetic energy becomes similar to the classical conservation of energy with an additional term representing the impact of the rotation on the dissipation of energy. Figure 3 compares the single energy decay route in NS [c.f. Eq. (39) and Fig. 3(a)] and the multiple routes proposed by MCT [c.f. Eq. (36) and Fig. 3(b)].

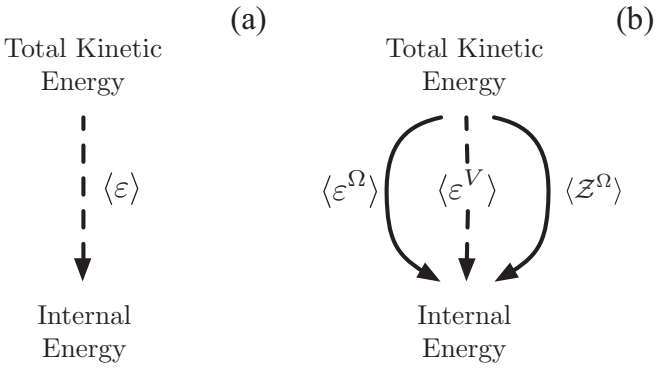

FIG. 3. Global total kinetic energy decay in (a) Navier-Stokes and (b) morphing continuum.

IV. NUMERICAL SIMULATION OF HOMOGENEOUS ISOTROPIC TURBULENCE

The present work is based on simulations of homogeneous isotropic turbulence in a triply periodic box. The reference case is taken from Ooi *et al.* [17] with Taylor-Reynolds number $\mathrm{Re}_\lambda = 70.9$ and Kolmogorov length scale $\eta = 2.3 \times 10^{-2}$. The aim of the current work is to reproduce Ooi's Navier-Stokes (NS) work in the presented morphing continuum framework (MCT) framework, and explore the energy cascade phenomena. The current study utilizes the small-scale structures to capture the small-scale turbulent structures or smallest eddies. This approach enables a clear insight into the effect of the translational and rotational motion of the small-scale eddies on the energy cascade phenomena.

To accomplish the above task, the current section is divided into three parts. In the first part, a model that gives meaning to the material parameters is presented. The model is implemented to translate a NS-based HIT case into the presented framework. Afterwards, the study presents the details of the numerical simulation. In the final section, the study assess the accuracy of the proposed model. The study compares the turbulent characteristic of both cases and evaluates whether the small-scale structures are capturing the smallest eddies in the flow.

A. Advanced kinetic theory

The difficulty in simulating a NS case in the MCT framework comes from estimating the value of the new dimensionless parameters that are not present in the classical theory (Er_λ, $C_\lambda^{\alpha\beta}$, C_λ^{γ}, $\mathcal{D}$). For this reason, the current study employs the work of Chen [42] and Wonnell and Chen [25] to give a kinetic description for the new material properties. The study by Wonnell and Chen shows that the only parameters that contribute to the viscous forces in MCT are the rotational viscosity (κ) and the gyrational diffusion (γ). Both of them are related by the equation $\gamma = \frac{3}{2} j\kappa$. From these definitions, two of the dimensionless parameters can be represented in terms the Taylor-Reynolds number as

$$C_\lambda^{\alpha\beta} = 0, \quad \mathrm{Er}_\lambda = \mathrm{Re}_\lambda, \quad C_\lambda^{\gamma} = \frac{\mathrm{Re}_\lambda}{3}. \tag{40}$$

B. Details of the NS and MCT numerical simulations

The simulation domain spans a distance of $2\pi \approx 273\eta$ in all directions. For the current case, isotropic forcing is achieved by adding energy into the linear momentum balance law only (i.e., $L_m = 0$). Different methods for injecting energy into low wave numbers have been described in the literature [43–45]. The linear momentum forcing implemented in the current study is similar to the work of Eswaran *et al.* [43] and Ooi *et al.* [17]. The energy inserted in the domain is added in the form of low wave number Fourier modes ($k \leqslant 2\sqrt{2}$) as a forcing term in the linear

TABLE I. Numerical and flow parameters for the two cases that are implemented or measured in this study.

Case	μ	κ	γ	j	λ	η	τ	$\mathcal{D}$
NS	0.025	0	0	–	0.38	0.023	0.21	–
MCT	0	0.05	1.8×10^{-5}	2.4×10^{-4}	0.38	–	–	3

momentum equation of the MCT balance laws. A Wiener statistical process is used to increment forcing in each time step. The forcing is projected onto a plane normal to the wave vector to ensure incompressibility.

The statistical quantities that are calculated at each time step are based on the three-dimensional translational energy spectrum E_v,

$$\frac{1}{2}v_i v_i = \int_0^\infty E_v(k)dk, \tag{41}$$

where the r.m.s. velocity is

$$v_{\text{rms}}^2 = \frac{2}{3}\int_0^\infty E_v(k)dk, \tag{42}$$

and the integral length scale is

$$L = \frac{\pi}{2v_{\text{rms}}^2}\int_0^\infty \frac{E_v(k)}{k}dk. \tag{43}$$

The other statistical quantities that are calculated only for the Navier-Stokes reference case is the Kolmogorov scale, i.e.,

$$\eta = \left(\frac{\nu^2}{2\int_0^\infty k^2 E_v(k)dk}\right)^{1/4}, \tag{44}$$

and the eddy turnover time is [6]

$$\tau = \frac{L}{v_{\text{rms}}}. \tag{45}$$

Table I summarizes the characteristics of the two different cases. The first case [17] is used as a reference case for the universal features of turbulence [16]. The second case represents a replica of the reference case but in the proposed framework. The diameter of the small-scale structure in case 2 is taken to be equal to the mesh size $d = 2\pi/128$, which is about seven times smaller than the Taylor microscale. This signifies that the small-scale structures are capturing eddies that are seven times smaller than the Taylor microscale.

Both cases are run sufficiently long (∼200 eddy turnover times) for the instantaneous energy spectra and other integral characteristics to become statistically steady. It may not be long enough for the large scales to reach statistical steadiness, but enough for the small scales. To ensure the simulation reached a steady-state solution, the temporal evolution of the volume-averaged total kinetic energy ($\frac{1}{2}v_i v_i + \frac{1}{2}j\omega_i\omega_i$) is plotted in Fig. 4. The transient phase took around 10 large-eddy turnover times, while the steady-state solution was run for 200 large-eddy turnover times. One interesting observation from Fig. 4, is that both cases show a similar trend in the instantaneous mean kinetic energy. If the steady-state data are averaged temporally, then the values are very close to each other (NS, 16.52 ± 2.57; MCT, 16.42 ± 2.72). As for the lag between the peaks of the data, it can be attributed to the time constant derived in the conservation of angular momentum in Sec. III.

The translational kinetic energy spectra, shown in Fig. 5(a), are averaged both spatially and temporally after the flow reaches a steady solution. The wave numbers shown in Fig. 5(a) are

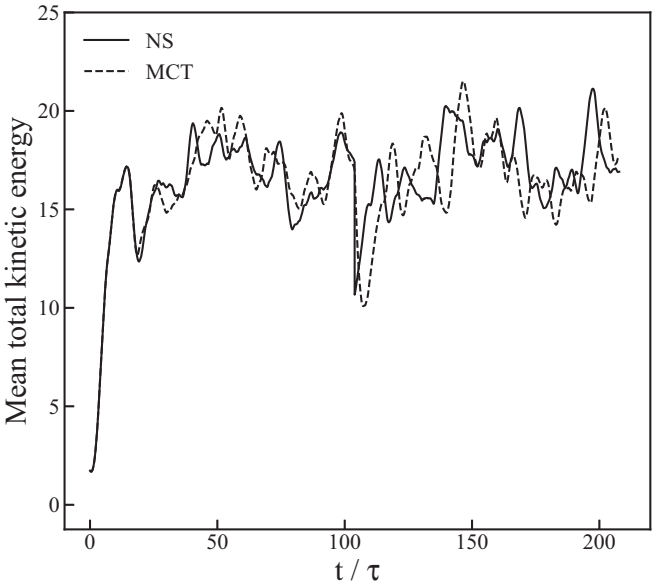

FIG. 4. Time evolution of the total mean kinetic energy.

normalized by the Kolmogorov scale obtained from the reference case. The figure confirms that the $-5/3$ Kolmogorov power-law slope exists for the total energy spectrum of the two cases around the integral scale.

The skewness (F_3) and kurtosis (F_4) of the x component of the velocity are plotted in Fig. 5(b) for all four cases to ensure homogeneity. The F_n operator is defined as [17]

$$F_n(v_\alpha) = (-1)^n \frac{\langle v_\alpha^n \rangle}{\langle v_\alpha^2 \rangle^{n/2}}, \tag{46}$$

where v_α is any one component of the velocity. Figure 5(b) shows that the kurtosis of the velocity remains constant at $\sim$2.85, which agrees with the kurtosis value reported by Batchelor's experimental data of grid turbulence [6]. The skewness of the velocity remained approximately zero throughout the computational time, in accordance with Batchelor [6].

C. Validation for the morphing continuum theory

After confirming that both cases have the same kinetic energy at the global scale, and that the simulation results are homogeneous, the next objective is to assess the feasibility of the proposed framework in two folds. The first objective is to evaluate the degree to which the small-scale structures are capturing the smallest eddies in the flow. Second, compare the turbulent features of the presented case with the reference case.

Figure 6 maps the joint probability distribution function (pdf) of the magnitude of the vorticity squared versus the magnitude of the gyration squared. The figures shows that highest concentration for the gyration is along the line, $\nabla \times v = 2\omega$, which indicates that most of the small-scale MCT structures are rotating at the same speed as the smallest eddies. Therefore, analyzing the gyration of the flow is equivalent to analyzing the rotational speed of the smallest eddy. The small-scale MCT structures can be used to capture the smallest turbulent structures (eddies) in the flow.

The next objective is to reproduce the invariant maps of Soria *et al.* [46], and show that both cases are able to generate the universal features of turbulence [16]. A brief review of the invariants

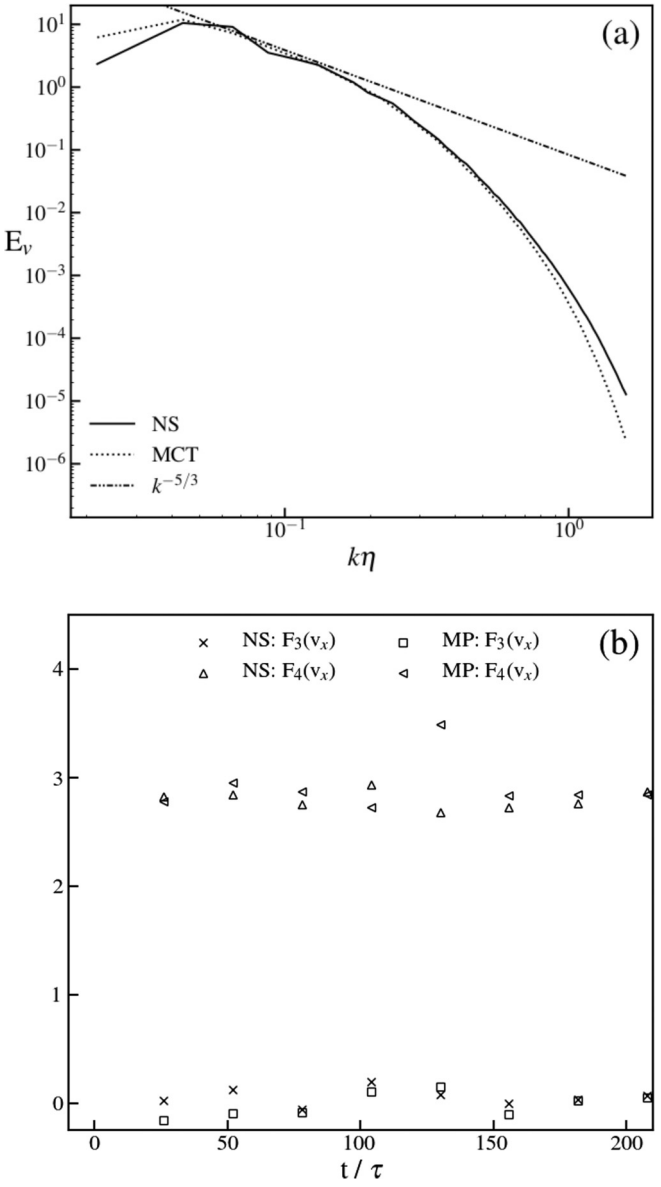

FIG. 5. The comparison of (a) three-dimensional translational kinetic energy spectra for the two cases and (b) time evolution of the skewness and kurtosis of the x component of the velocity for the four cases.

employed in the classical fluid theory and their derivation is given first, followed by an analysis of the invariant maps for both cases.

The deformation gradient in the classical fluid theory is the velocity gradient tensor $v_{l,k}$, which can be split into a symmetric and skew-symmetric tensors,

$$v_{l,k} = S_{kl} + \Omega_{kl}, \tag{47}$$

where S_{kl} is the *strain rate tensor* defined as

$$S_{kl} = \tfrac{1}{2}(v_{l,k} + v_{k,l}), \tag{48}$$

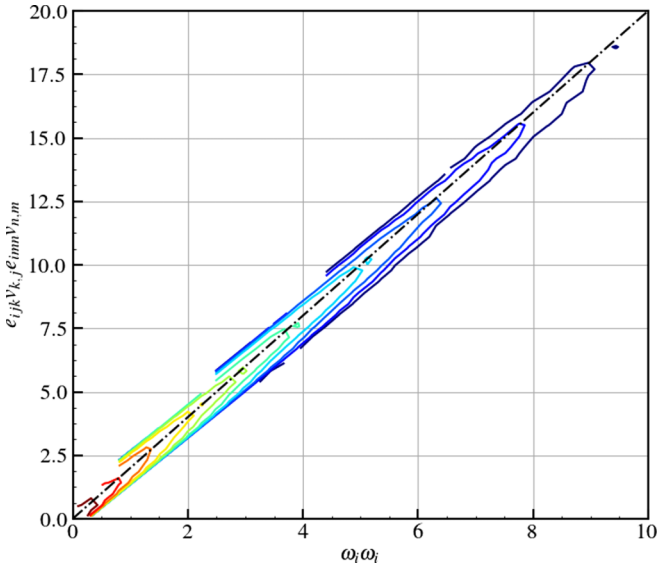

FIG. 6. Joint pdf of the magnitude of the vorticity squared vs the magnitude of the gyration squared. The colors correspond to the value of the joint pdf (red, 10^{-5}; violet, 0.1).

and Ω_{kl} is the *spin rate tensor* defined as

$$\Omega_{kl} = \tfrac{1}{2}(v_{l,k} - v_{k,l}). \tag{49}$$

The characteristic equation that satisfies the eigenvalue equation for the velocity gradient tensor is

$$\lambda_i^3 + P\lambda_i^2 + Q\lambda_i + R = 0, \tag{50}$$

where λ_i is the eigenvalues of $v_{k,l}$, and P, Q, and R are the first, second, and third invariants of $v_{k,l}$. The nature of the three roots of the characteristic equation helps identify the small-scale flow topology by varying in the form of four possibilities: (1) three distinct real roots; (2) two equal real roots and one different; (3) three equal real roots; and (4) one real root with two complex conjugate roots.

Instead of solving for the roots of the characteristic equation to infer the category of solution, Chong *et al.* [47] showed that by studying the properties of the three invariants P, Q, and R of the velocity gradient, one can infer the nature of the roots, and the topology of the flow. The first invariant P defined as

$$P = -\mathrm{tr}(v_{k,l}) = -v_{k,k} = -S_{kk}. \tag{51}$$

It represents the compressibility of the flow, thus vanishes for an incompressible flow. The second invariant Q for an incompressible flow is defined as

$$Q = \tfrac{1}{4}(\Omega_k\Omega_k - 2S_{kl}S_{kl}), \tag{52}$$

where $\Omega_k = e_{kml}v_{m,l}$ is the vorticity field. Q measures the relative straining and enstrophy ($\mathcal{Z}^v = \Omega_k\Omega_k/2$) experienced by a fluid element. The third invariant R for an incompressible flow is defined as

$$R = -\tfrac{1}{3}v_{k,l}v_{l,m}v_{m,k} = -\tfrac{1}{3}\left(S_{kl}S_{lm}S_{mk} + \tfrac{3}{4}\Omega_k\Omega_l S_{kl}\right). \tag{53}$$

It measures the relative strain production or amplification ($S_{ij}S_{jk}S_{ki}$) over the enstrophy production term ($\Omega_i\Omega_j S_{ij}$). A similar decomposition for the invariants of the velocity gradient is used on the strain rate tensor, S_{kl}, and the spin rate tensor, Ω_{kl}. The invariants of the rate-of-strain tensor S_{kl} are

$$P_S = -\mathrm{tr}(S_{lk}) = -v_{k,k}, \tag{54}$$

$$Q_S = -\tfrac{1}{2}S_{kl}S_{lk}, \tag{55}$$

$$R_S = -\tfrac{1}{3}S_{ij}S_{jk}S_{ki}. \tag{56}$$

The second invariant Q_S is proportional to the small-scale rate of viscous dissipation of translational kinetic energy in both classical theory and morphing continuum theory. As for the third invariant R_S, it is proportional to the skewness of the strain rate and its production. The only nonzero invariant for Ω_{kl} is the second invariant,

$$Q_W = -\tfrac{1}{2}\Omega_{kl}\Omega_{lk} = \tfrac{1}{4}\Omega_m\Omega_m. \tag{57}$$

This invariant is proportional to half the enstrophy ($\mathcal{Z}^v$).

To validate the turbulence features of the MCT simulation, the three most common invariant maps of the presented simulation are compared with the reference simulation shown in Fig. 7. The invariants are normalized with $\langle S_{ij}S_{ij}\rangle$ following the work of Da Silva and Pereira [48]. The first invariant map that is analyzed is the second invariant of the velocity gradient tensor Q versus third invariant R. The classical (Q, R) diagram gives insight in to the nature of the flows small-scale topology (strain or enstrophy dominated), and the topology of the vortices (compression or expansion) [48]. The joint pdfs of R and Q for the both cases are shown in Figs. 7(a) and 7(b). The black dotted line represent the locus of points at which $D = 0$, where D is the discriminant [47], and for an incompressible flow its defined as

$$D = \tfrac{27}{4}R^2 + Q^3. \tag{58}$$

Figure 7(a), which refers to the reference case, and Fig. 7(b), which refers to the presented case, show a joint pdf, similar to the well-known universal teardrop diagrams of Ooi *et al.* [17]. This shape implies that the majority of the flow is enstrophy dominated ($Q > 0$) with a strong correlations between the vortex stretching part ($R < 0$) and the vortex compression part ($R > 0$). An interesting observation from both figures, is that the invariants of the presented case show to a high proximity the same distribution and magnitude as the invariants of the reference case.

Another classical invariant map implemented in the study of the topology of the flow is the (R_S, Q_S) map. The importance of this map lies in its ability to analyze the geometry of the small-scale straining of the fluid element. In particular, the third invariant R_S is associated with the strain production [48]. A negative R_S indicates a region undergoing intense contraction and destruction of the strain product, and a positive R_S implies regions of high expansion, and production of the strain product. Figures 7(c) and 7(d) show the joint pdfs of the (R_S, Q_S) invariant maps for both cases. The two joint pdfs are identical, and show a clear preference for the region where R_S is greater than zero. It indicates that most of the flow is experiencing regions of intense expansion of the fluid element, while only a few regions are experiencing compression.

The third invariant map is the ($-Q_S$, Q_W) map, analyzes the dissipation of translational kinetic energy. Points close to the horizontal line (Q_W) represents regions at the center of the vortex tubes that have high enstrophy ($\mathcal{Z}^v$) but small translational dissipation (ε^v). However, points close to the vertical line ($-Q_S$) represents regions away from the vortex tubes with high translational dissipation but low enstrophy. Figures 7(e) and 7(f) confirm the observations previously made on the topology of the flow in each case. The figures show a joint pdf similar to the work done on isotropic turbulence by Ooi *et al.* [17], with no desirable tendency for the flow to be aligned near the horizontal or vertical lines.

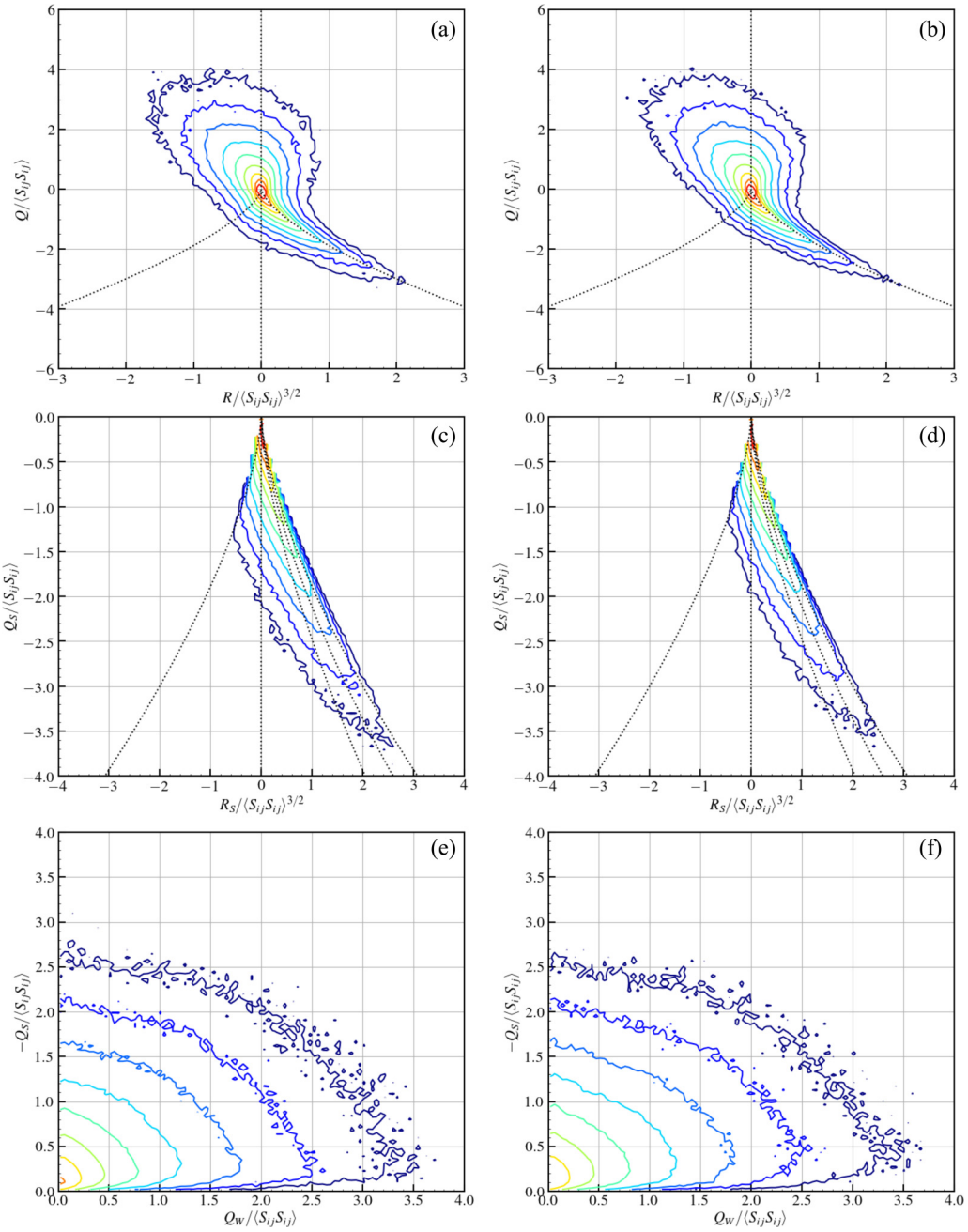

FIG. 7. Joint pdfs of the invariants maps of (Q, R), (Q_S, R_S), and $(-Q_S, Q_W)$ for both cases: (a, c, e) for the NS case and (b, d, f) for the MCT case. Each map contains seven colors, which correspond to different joint pdfs. All invariants are normalized by $\langle S_{ij}S_{ij}\rangle$.

The current section shows that the proposed methodology is not only capable of replicating the turbulence characteristics of an NS simulation at the global scale, but also capable of replicating the topological features of turbulence at the small scale.

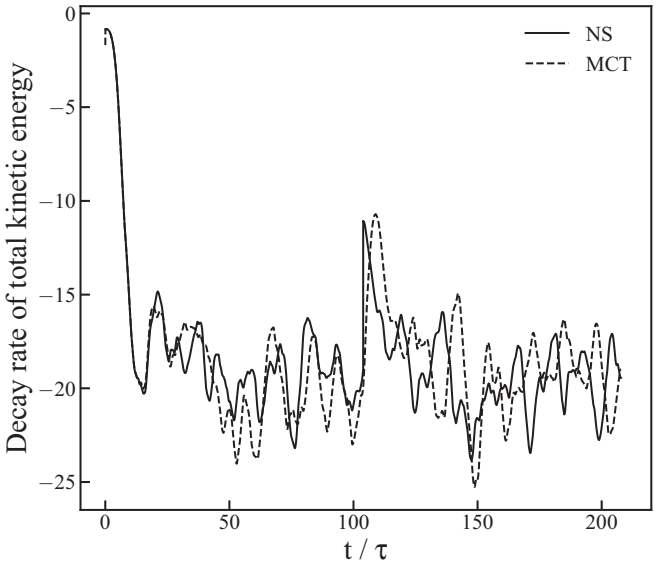

FIG. 8. Temporal evolution of the decay rate of the total kinetic energy $(\frac{d}{dt}\langle\frac{1}{2}v_i v_i\rangle + \langle\frac{1}{2}j\omega_i\omega_i\rangle)$.

V. ENERGY ANALYSIS

The energy routes are employed to investigate the flow of energy in homogeneous isotropic turbulence. The analysis begins by investigating these energy routes at the global scale, followed by an analysis at the small scale. In Sec. III, six routes that control the energy flow were derived; two for the translational kinetic energy (ε^v and $\mathcal{T}^v$) and four for the rotational kinetic energy ($\varepsilon^\omega_\gamma$, $\varepsilon^\omega_{\alpha\beta}$, δ^ω, and $\mathcal{T}^\omega$). These routes were found to be dependent on the translational velocity v_i and the gyration of the small-scale structures ω_i. However, Sec. IV shows that the majority of the small-scale structures are capturing the smallest eddy characterized by vorticity, i.e., $\omega_i \approx \frac{1}{2}\varepsilon_{ijk}v_{k,j}$. Thus, the five active energy routes ($\varepsilon^\omega_{\alpha\beta} = 0$) can be written in term of the translational velocity v_i only.

A. Energy transfer at the global scale

The mean value of the newly derived energy routes are investigated in this section. The analysis sheds light on the similarities between the classical energy route and newly derived energy route. In the classical fluid theory, the only component that contributes to the change of the mean kinetic energy is the mean dissipation term $\langle\varepsilon\rangle$. In the presented framework, there are six components that contribute to the change of the mean total kinetic energy [Eq. (35)]. However, if the gyration is equivalent to the rotational speed of the fluid element ($\frac{1}{2}\varepsilon_{ijk}v_{k,j}$), then the six components can be reduced to two components one of them similar to the classical dissipation term as shown in Eq. (39).

The mean decay rate of the total kinetic energy of the box turbulence study cases is shown in Fig. 8. The figure shows that both reference and presented cases are decaying almost identical amount of total kinetic energy on a global scale (NS, 20.4 ± 3.2; MCT, 20.3 ± 3.4). The plot strengthen the earlier observation, that the two cases are not only experiencing the same trend in total kinetic energy but also similar decay rates.

To understand the detailed energy loss in the homogeneous isotropic turbulence, the total kinetic energy is decoupled into the translational kinetic energy field $\frac{1}{2}v_i v_i$, and the rotational kinetic energy field $\frac{1}{2}j\omega_i\omega_i$. Figures 9(a) and 9(b) plot the temporal evolution of the components responsible for the change in translational or rotational kinetic energy. The sign of the plot is based on whether the

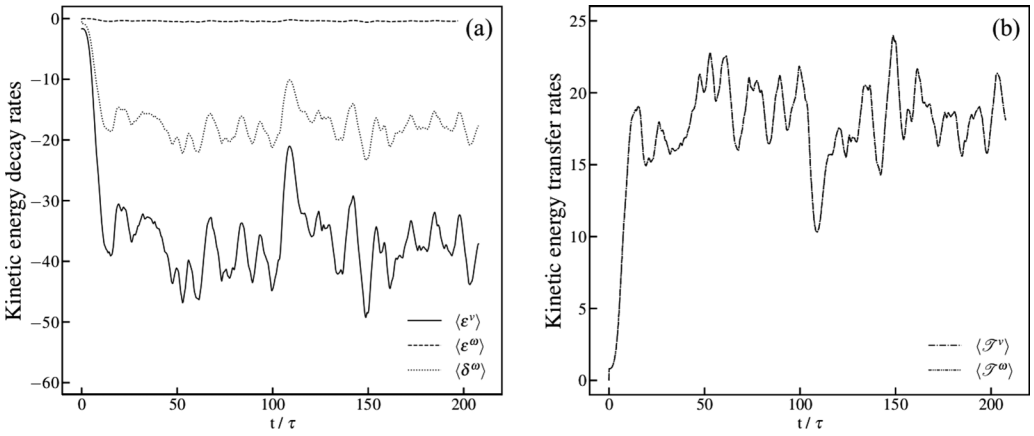

FIG. 9. Temporal evolution of the components responsible rate of change of the translational and rotational kinetic energy: (a) mean translational dissipation $\langle \varepsilon^v \rangle$, mean rotational dissipation $\langle \varepsilon^\omega \rangle$, and mean rotational decay $\langle \delta^\omega \rangle$; (b) mean translational transfer rate $\langle \mathcal{T}^v \rangle$, and mean rotational transfer rate $\langle \mathcal{T}^\omega \rangle$.

component is causing a loss or gain in kinetic energy, i.e., a negative value implies a loss of kinetic energy, and a positive value implies a gain of kinetic energy. It should be noted that the summation of temporal evolution in Figs. 9(a) and 9(b) yields the total kinetic energy decay rate shown in Fig. 8.

Figure 9(a) plots the evolution of the components responsible for the dissipation and decay of kinetic energy; the mean translational dissipation ($\langle \varepsilon^v \rangle$), the mean rotational dissipation ($\langle \varepsilon^\omega \rangle$), and the mean rotational decay rate ($\langle \delta^\omega \rangle$). Figure 9(b) plots the evolution of the components responsible for the transfer of kinetic energy; translational transfer rate ($\langle \mathcal{T}^v \rangle$) and rotational transfer rate ($\langle \mathcal{T}^\omega \rangle$). Figure 9(b) shows that the sign of the evolution of the transfer rates is positive, unlike the sign of the evolution of the dissipation or decay rates [Fig. 9(a)]. This implies that $\langle \mathcal{T}^v \rangle$ and $\langle \mathcal{T}^\omega \rangle$ are not dispersing kinetic energy, but are injecting kinetic energy into the system. This behavior indicates a new type of inverse energy cascade. One should note that $\mathcal{T}^v$ and $\mathcal{T}^\omega$ do not take energy from the small scale and give it to the large scale, like the conventional notation for inverse cascade. Instead, they take energy from the internal energy and gives it to the system as a whole. This energy can either go from the small scales to the large scales as the conventional inverse cascade or stay at the small scales and dissipate into heat as the classical forward cascade.

Adding the two components responsible for the change in translational kinetic energy $\langle \mathcal{T}^v \rangle$ and $\langle \varepsilon^v \rangle$ yields a mean dissipative rate equivalent to the one shown in Fig. 8. Although MCT seems to dissipate more translational kinetic energy than the classical theory, this larger loss is compensated by the energy taken from the internal energy by $\mathcal{T}^v$. As for the rotational energy, comparing the temporal evolution of $\langle \mathcal{T}^\omega \rangle$, with $\langle \varepsilon^\omega \rangle$, one sees that they are identical. Thus, the lose in rotational kinetic energy due to $\langle \delta^\omega \rangle$ is accompanied by an increase in kinetic energy gain through the transfer component $\langle \mathcal{T}^\omega \rangle$. Resulting in an average rate of change of rotational kinetic energy to be very close to zero. Thus, the energy gained by the rotational kinetic energy is equal to the energy lost by it. In other words, the conservation of rotational kinetic is achieved at the global scale, which implies a conservation of angular momentum, i.e., $\langle \omega \rangle = 0$.

B. Energy transfer at the small scale

The previous section investigated the energy routes on global scale, i.e., mean throughout the domain. The current section instigates the same routes but on the local scale. However, since the MCT small-scale structure is seven times smaller than the Taylor microscale, the local scale is close to the small-scale turbulent structures. Thus, the investigation at the local scale is equivalent to that at the turbulent small scale. In addition, since the results have already reached a statistical steady

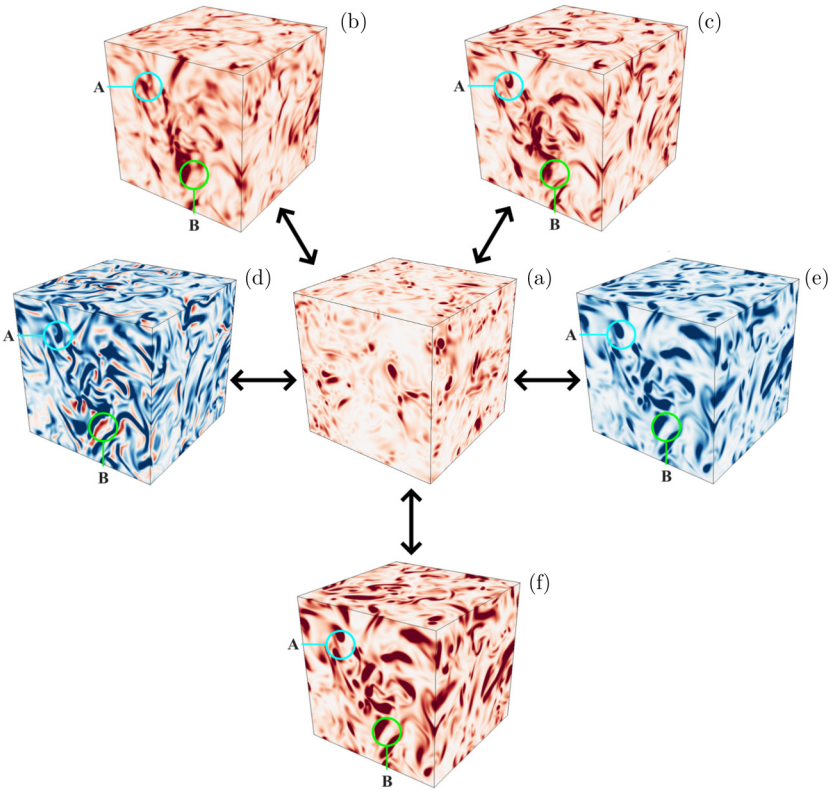

FIG. 10. Snapshot of the instantaneous isolines depicting the small-scale components responsible for the rate of change of kinetic energy: (a) energy dissipation for the NS case ε, (b) translational dissipation ε^{v}, (c) rotational dissipation $\varepsilon^{\omega}_{\gamma}$, (d) translational transfer rate $\mathcal{T}^{v}$, (e) rotational transfer rate $\mathcal{T}^{\omega}$, and (f) rotational decay δ^{ω}.

state, one can investigate the instantaneous behavior of the energy routes, and assume it is the same through out the full elapsed steady-state time. Figures 10(a)–10(f) plots the instantaneous isolines of the components responsible for the change in the kinetic energy in the MCT and NS cases. The color of the plot is based on whether the component is causing a loss or a gain in kinetic energy; a red color implies a loss, and a blue color implies a gain of kinetic energy. The isolines are normalized by the instantaneous mean value for each component.

Figure 10(a) plots the isolines for the dissipation rate of kinetic energy from the case (ε). Figures 10(b)–10(f) plot the isolines for the components responsible for the change of kinetic energy in the presented case. Figures 10(b), 10(c), and 10(d) plot the isolines for the components responsible for the decay of total kinetic energy; translation dissipation (ε^{v}), rotational dissipation (ε^{ω}), and rotational decay rate (δ^{ω}), respectively. Figures 10(d) and 10(e) plot the isolines for the components responsible for injecting or ejecting kinetic energy ($\mathcal{T}^{v}$ and $\mathcal{T}^{\omega}$). The isolines for those two figures are mostly colored blue indicating that they are causing a new type of inverse energy cascade (energy flow from internal to kinetic). On the global scale, $\langle\mathcal{T}^{\omega}\rangle$ and $\langle\mathcal{T}^{v}\rangle$ were shown to be equal as shown in Fig. 9(b). On the small scale, however, it is a different story. Section III shows that on the small scale $\mathcal{T}^{\omega}$ and $\mathcal{T}^{v}$ are related through the equation

$$\frac{\kappa}{\rho}(\varepsilon_{mln}\omega_l v_n)_{,m} = \mathcal{T}^{v} - \mathcal{T}^{\omega}, \tag{59}$$

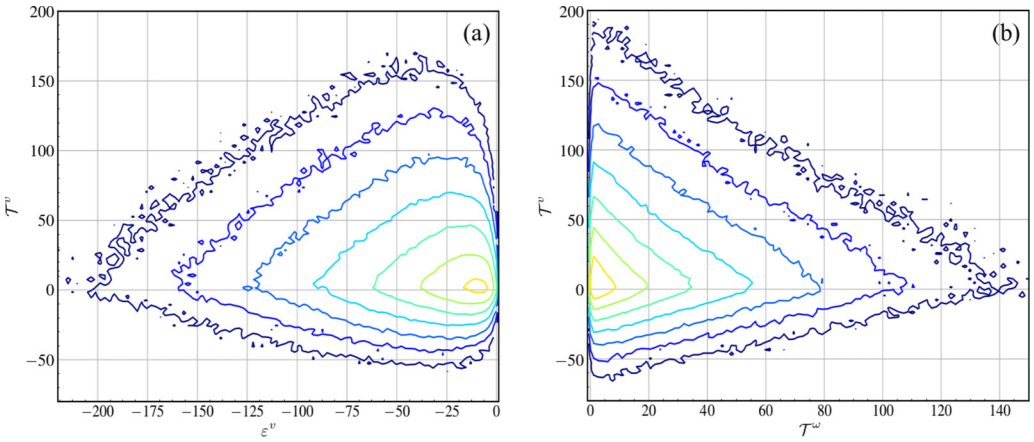

FIG. 11. Joint pdf of the energy routes. (a) $(\mathcal{T}^v, \varepsilon^v)$ and (b) $(\mathcal{T}^v, \mathcal{T}^\omega)$.

where the mean average of $(\varepsilon_{mln}\omega_l v_n)_{,m}$ is zero. Figures 10(d) and 10(e), which refer to $\mathcal{T}^v$ and $\mathcal{T}^\omega$, respectively, show that these two terms never inject kinetic energy in the same location at the same time. At a single location, either rotational kinetic energy is injected by $\mathcal{T}^\omega$ or translational kinetic energy is injected by $\mathcal{T}^v$. Zone A, in Fig. 10(d), shows a blue spot in the middle surrounded by white lines indicating a gain in translational kinetic energy. However, zone A in Fig. 10(e) shows a white in the middle indicating no transfer of energy. This implies that at the small scale, points with high value of $\mathcal{T}^v$ have almost a null value of $\mathcal{T}^\omega$, and vice versa. This phenomena is clearly explained in the joint pdf of the energy routes shown in Fig. 11. The only way for $\mathcal{T}^v$ and $\mathcal{T}^\omega$ to be equal on the small scale is for $(\varepsilon_{mln}\omega_l v_n)_{,m}$ to be zero. One possible scenario is to have the velocity (v_n) and the axis at which the gyration (ω_n) is rotating to be parallel to each other. This case can only occur when the rotational motion of the small-scale structures decouples from the translational motion.

Comparing Figs. 10(e) and 10(f) for $\mathcal{T}^\omega$ and δ^ω, one can see that the isolines are similar but their colors are different. This proves that the rotational decay (δ^ω) and the rotational transfer rate $(\mathcal{T}^\omega)$, are equivalent at the global and small scales but with an inverted function. This can be easily proved by going back to the definition of both routes and noting that $\omega_i \approx \frac{1}{2}\varepsilon_{ijk}v_{k,j}$,

$$\mathcal{T}^\omega = \frac{\kappa}{\rho}\omega_m(\varepsilon_{mln}v_{n,l}) \approx \frac{\kappa}{2\rho}\varepsilon_{mjk}v_{k,j}\varepsilon_{mln}v_{n,l}, \tag{60}$$

$$\delta^\omega = 2\frac{\kappa}{\rho}\omega_m\omega_m \approx \frac{\kappa}{2\rho}\varepsilon_{mjk}v_{k,j}\varepsilon_{mln}v_{n,l}. \tag{61}$$

Thus, any point that is experiencing a decay in the rotational kinetic energy also experiences an equivalent gain in the rotational kinetic energy so that the mean rotational kinetic energy is kept constant. This behavior indicates that the conservation of the angular momentum at both the global and small scale is conserved, i.e., the rate of change of the small-scale gyration equals zero $(d\omega/dt = 0)$.

Out of the six isolines shown in Fig. 10, only Fig. 10(d), which is for $\mathcal{T}^v$, is showing both forms of energy transfer as evident in zones A and B. Thus, $\mathcal{T}^v$ is the only term that is showing both forms of energy cascade. To understand the dual function of $\mathcal{T}^v$ in providing or dissipating energy one has to look at the kinematics of the small-scale structures. Figure 2(a) shows that if the curl of the gyration $(\nabla \times \vec{\omega})$ is generating a translational motion along the direction of the velocity (i.e., $\alpha < 90$), energy is injected into the translational motion. However, if the resultant translation motion created by the curl of the gyration is opposing the velocity of the small-scale structure, the translational energy is lost as heat. Going back to Fig. 10, one can see that the dominant behavior for the curl of the gyration and the velocity to be aligned in the same direction. In some cases, the curl of the gyration and the velocity are against each other. This occurs when the small-scale structures

suddenly shift their translational direction and move in a completely opposite manner. One reason for this is due to absorbing so much translational kinetic energy in a small duration of time and not allowing the gyration enough time to adjust to it.

To gain more insight into the relation between the energy routes, the joint pdf of the routes are plotted in Fig. 11. Figure 11(a) plots the joint pdf of ($\mathcal{T}^v$, ε^v), while Fig. 11(b) plots the joint pdf of ($\mathcal{T}^v$, $\mathcal{T}^\omega$). Figure 11(a) shows that highest absolute levels of dissipation "$|\varepsilon^v|$" occurs in locations where the translational transfer rate "$\mathcal{T}^v$" is almost null. The figure also shows that that regions experiencing the highest $|\mathcal{T}^v|$ are accompanied by the lowest values for $|\varepsilon^v|$. It Indicates that at the small scale, the two routes $\mathcal{T}^v$ and ε^v are inversely proportional. Figure 11(b) reveals a similar relationship between the two transfer routes $\mathcal{T}^v$ and $\mathcal{T}^\omega$. The highest levels in rotational transfer rate "$\mathcal{T}^\omega$" occurs in locations where the translational transfer rate "$\mathcal{T}^v$" is almost null, and vice versa. Even though the two transfer routes are equivalent at the global scale, locally they are inversely proportional. The figure shows that at the small scale only one route can dominant the flow of the energy, with the deciding factor lies with the kinematics of the small scales.

VI. CONCLUSION

The current paper addresses the energy flow in homogeneous isotropic turbulence (HIT) from the perspective of a completely decoupled rotational and translational motions. The paper begins by presenting the incompressible balance laws for MCT in their dimensional and dimensionless form, and explains the meaning behind the new dimensionless parameters. The conservation laws for linear momentum, angular momentum and energy are then derived. The laws show similarities between the morphing continuum theory and the classical Navier-Stokes in conservation of linear momentum, but they show differences in the conservation of angular momentum. It shows a new time constant τ^ω that represents the characteristic time for the angular momentum to reach equilibrium, and links the derived time constant with the time constant of the extended Boltzmann equation [41]. The conservation of energy shows that by segregating the kinetic energy into its rotational and translational components, one can realize new energy routes not found in the classical theory. In particular, the conservation law for the translational kinetic energy shows, in addition to the classical dissipation route (ε^v), a new transfer route ($\mathcal{T}^v$) that could inject or eject energy. As for the conservation law for the rotational kinetic energy they posses their own routes; one route that dissipates energy (ε^ω), one route that decays it (δ^ω), and one transfer route ($\mathcal{T}^\omega$) that could inject or eject energy in it. The new transfer routes show that internal energy can be converted into rotational or translational kinetic energy depending on the kinematics of the small-scale rotation and translation.

The conservation laws are later employed in Ooi *et al.*'s [17] HIT study. The study begins by presenting a model to reproduce the Navier-Stokes case into the presented framework, followed by a comparison of both cases to assess the accuracy of the proposed model. The two cases show similar results on the global scale by having equivalent mean kinetic energy and on the small scale by agreeing to Kolmogorov 5/3 law. In addition, the two cases show similarities in joint pdfs of the invariants of the velocity gradient indicating similar turbulent characteristics at all scales. Finally, the study implements these routes to investigate the flow of energy. The study shows on the global scale, sum of the energy routes is equivalent to the single classical dissipation route in NS. If divided up, however, then the study shows that out of the six energy routes, two transfer routes are injecting kinetic energy into the flow while the rest are dissipating energy. On the small scale, the study shows that the relation between the rotational and translational motions of the small scales affect the flow of energy through the translation transfer rate ($\mathcal{T}^v$). If the translational velocity and the curl of the rotational velocity (ω) are aligned, the $\mathcal{T}^v$ causes a gain in kinetic energy. However, if the two motions are misaligned by more than 90°, $\mathcal{T}^v$ will dissipate kinetic energy. Finally, the study analysis the joint pdfs of the three dominant routes ($\mathcal{T}^v$, $\mathcal{T}^\omega$, and ε^v). The study shows that at the global scale $\mathcal{T}^v$ and $\mathcal{T}^\omega$ are equal, but on the small scale they are inversely proportional.

ACKNOWLEDGMENT

This material is based upon work supported by the Air Force Office of Scientific Research under Award No. FA9550-17-1-0154.

[1] K. R. Sreenivasan and R. Antonia, The phenomenology of small-scale turbulence, Annu. Rev. Fluid Mech. **29**, 435 (1997).
[2] P. Bechlars and R. D. Sandberg, Variation of enstrophy production and strain rotation relation in a turbulent boundary layer, J. Fluid Mech. **812**, 321 (2017).
[3] M. Lesieur and O. Metais, New trends in large-eddy simulations of turbulence, Annu. Rev. Fluid Mech. **28**, 45 (1996).
[4] C. G. Speziale, Turbulence modeling for time-dependent RANS and VLES: a review, AIAA J. **36**, 173 (1998).
[5] K. Mahesh, G. Constantinescu, and P. Moin, A numerical method for large-eddy simulation in complex geometries, J. Comput. Phys. **197**, 215 (2004).
[6] G. K. Batchelor, *The Theory of Homogeneous Turbulence* (Cambridge University Press, Cambridge, 1953).
[7] G. I. Taylor, Production and dissipation of vorticity in a turbulent fluid, Proc. R. Soc. London A **164**, 15 (1938).
[8] R. Betchov, An inequality concerning the production of vorticity in isotropic turbulence, J. Fluid Mech. **1**, 497 (1956).
[9] A. N. Kolmogorov, The local structure of turbulence in incompressible viscous fluid for very large Reynolds numbers, Proc. Math. Phys. Sci. **434**, 9 (1991).
[10] U. Frisch, *Turbulence: The Legacy of A. N. Kolmogorov* (Cambridge University Press, Cambridge, 1995).
[11] L. M. Zubair, Studies in turbulence using wavelet transforms for data compression and scale separation, Ph.D. thesis, Yale University, 1994.
[12] A. Vincent and M. Meneguzzi, The dynamics of vorticity tubes in homogeneous turbulence, J. Fluid Mech. **258**, 245 (1994).
[13] J. Jimenez and A. A. Wray, On the characteristics of vortex filaments in isotropic turbulence, J. Fluid Mech. **373**, 255 (1998).
[14] K. Horiuti, A classification method for vortex sheet and tube structures in turbulent flows, Phys. Fluids **13**, 3756 (2001).
[15] J. Chen, Morphing continuum theory for turbulence: Theory, computation, and visualization, Phys. Rev. E **96**, 043108 (2017).
[16] J. M. Chacin and B. J. Cantwell, Dynamics of a low Reynolds number turbulent boundary layer, J. Fluid Mech. **404**, 87 (2000).
[17] A. Ooi, J. Martin, J. Soria, and M. S. Chong, A study of the evolution and characteristics of the invariants of the velocity-gradient tensor in isotropic turbulence, J. Fluid Mech. **381**, 141 (1999).
[18] A. C. Eringen, *Microcontinuum Field Theories: I. Foundations and Solids* (Springer Science & Business Media, Berlin, 2001), Vol. 1.
[19] A. C. Eringen, *Microcontinuum Field Theories: II. Fluent media* (Springer Science & Business Media, Berlin, 2001), Vol. 2.
[20] A. C. Eringen, Simple microfluids, Int. J. Eng. Sci. **2**, 205 (1964).
[21] J. S. Hansen, P. J. Daivis, J. C. Dyre, B. Todd, and H. Bruus, Generalized extended Navier-Stokes theory: Correlations in molecular fluids with intrinsic angular momentum, J. Chem. Phys. **138**, 034503 (2013).
[22] A. C. Eringen, Theory of micropolar fluids, J. Math. Mech. **16**, 1 (1966).
[23] A. C. Eringen, Theory of thermomicrofluids, J. Math. Anal. Appl. **38**, 480 (1972).
[24] S. R. De Groot and P. Mazur, *Non-equilibrium Thermodynamics* (Dover Publications, Mineola, NY, 2013).

[25] L. B. Wonnell and J. Chen, First-order approximation to the Boltzmann-Curtiss equation for flows with local spin, J. Eng. Math. **114**, 43 (2019).
[26] I. Papautsky, J. Brazzle, T. Ameel, and A. B. Frazier, Laminar fluid behavior in microchannels using micropolar fluid theory, Sensors Actuat. A: Phys. **73**, 101 (1999).
[27] J. Prakash and P. Sinha, Lubrication theory for micropolar fluids and its application to a journal bearing, Int. J. Eng. Sci. **13**, 217 (1975).
[28] K. S. Mekheimer and M. A. El Kot, The micropolar fluid model for blood flow through a tapered artery with a stenosis, Acta Mech. Sinica **24**, 637 (2008).
[29] L. Wonnell and J. Chen, Morphing continuum theory: Incorporating the physics of microstructures to capture the transition to turbulence within a boundary layer, J. Fluids Eng. **139**, 011205 (2017).
[30] L. Wonnell and J. Chen, *A Morphing Continuum Approach to Compressible Flows: Shock Wave-Turbulent Boundary Layer Interaction* (AIAA, Reston, VA, 2016), pp. 42–79.
[31] L. B. Wonnell and J. Chen, *Extension of Morphing Continuum Theory to Numerical Simulations of Transonic Flow Over A Bump* (AIAA, Reston, VA, 2017), pp. 34–61.
[32] M. I. Cheikh and J. Chen, *A Morphing Continuum Approach to Supersonic Flow Over a Compression Ramp* (AIAA, Reston, VA, 2017), pp. 34–60.
[33] J. Chen, C. Liang, and J. D. Lee, Numerical simulation for unsteady compressible micropolar fluid flow, Comput. Fluids **66**, 1 (2012).
[34] J. Chen, J. D. Lee, and C. Liang, Constitutive equations of micropolar electromagnetic fluids, J. Non-Newtonian Fluid Mech. **166**, 867 (2011).
[35] M. I. Cheikh, L. B. Wonnell, and J. Chen, Morphing continuum analysis of energy transfer in compressible turbulence, Phys. Rev. Fluids **3**, 024604 (2018).
[36] V. I. Arnold, Hamiltonian nature of the Euler equations in the dynamics of a rigid body and of an ideal fluid, in *Vladimir I. Arnold - Collected Works*, edited by A. Givental, B. Khesin, A. Varchenko, V. Vassiliev, and O Viro (Springer, Berlin, Heidelberg, 1969), Vol. 2, pp. 175–178.
[37] T. G. Shepherd, Symmetries, conservation laws, and Hamiltonian structure in geophysical fluid dynamics, Adv. Geophys. **32**, 287 (1990).
[38] Y. Kosmann-Schwarzbach, *The Noether Theorems* (Springer, New York, 2011).
[39] P. L. Bhatnagar, E. P. Gross, and M. Krook, A model for collision processes in gases. I. Small amplitude processes in charged and neutral one-component systems, Phys. Rev. **94**, 511 (1954).
[40] G. Wannier, *Statistical Mechanics* (John Wiley and Sons, New York, 1966).
[41] H. Chen, S. Kandasamy, S. Orszag, R. Shock, S. Succi, and V. Yakhot, Extended Boltzmann kinetic equation for turbulent flows, Science **301**, 633 (2003).
[42] J. Chen, An advanced kinetic theory for morphing continuum with inner structure, Rep. Math. Phys. **80**, 317 (2017).
[43] V. Eswaran and S. B. Pope, An examination of forcing in direct numerical simulations of turbulence, Comput. Fluids **16**, 257 (1988).
[44] E. D. Siggia and G. S. Patterson, Intermittency effects in a numerical simulation of stationary three-dimensional turbulence, J. Fluid Mech. **86**, 567 (1978).
[45] N. P. Sullivan, S. Mahalingam, and R. M. Kerr, Deterministic forcing of homogeneous, isotropic turbulence, Phys. Fluids **6**, 1612 (1994).
[46] J. Soria, R. Sondergaard, B. J. Cantwell, M. S. Chong, and A. E. Perry, A study of the fine-scale motions of incompressible time-developing mixing layers, Phys. Fluids **6**, 871 (1994).
[47] M. S. Chong, A. E. Perry, and B. J. Cantwell, A general classification of three-dimensional flow fields, Phys. Fluids **2**, 765 (1990).
[48] C. B. Da Silva and J. C. Pereira, Invariants of the velocity-gradient, rate-of-strain, and rate-of-rotation tensors across the turbulent/nonturbulent interface in jets, Phys. Fluids **20**, 055101 (2008).